

## Supporting Information

# High-Performance Metal-Iodine Batteries Enabled by Bifunctional Dendrite-Free LiNa Alloy Anode

*Donglin Yu, <sup>a, b</sup> Dong Liu, <sup>a</sup> Lei Shi, <sup>a, b</sup> Jieshan Qiu, <sup>\*a</sup> and Liming Dai <sup>\*c</sup>*

<sup>a</sup> State Key Laboratory of Organic–Inorganic Composites, Beijing Advanced Innovation Center for Soft Matter Science and Engineering, College of Chemical Engineering, Beijing University of Chemical Technology, Beijing, 100029, China.

<sup>b</sup> College of Materials Science and Engineering, Beijing University of Chemical Technology, Beijing, 100029, China.

<sup>c</sup> School of Chemical Engineering, University of New South Wales, Sydney, NSW2052, Australia.

\* Corresponding authors:

Emails: qiujs@mail.buct.edu.cn (JQ); l.dai@unsw.edu.au (LD)

## Experimental Section

**Preparation of LiNa-CC metal Electrodes.** Prior to prepare LiNa-CC metal anodes, the commercial carbon cloth (CC, HCP331N) was cleaned by O<sub>2</sub> and NH<sub>3</sub> plasma for 10 min, respectively. Commercial lithium foil and sodium piece with a molar ratio of 2:1 were melted at 320 °C in the glove box (H<sub>2</sub>O, O<sub>2</sub> < 0.1 ppm). After the Li and Na metal melting into liquid alloy phase, the carbon cloth (CC, 12 mm discs) was immersed into the liquid immediately. The LiNa liquid alloy can be uniformly loaded on the CC in less than 10 seconds. The LiNa-CC with various Li/Na molar ratios of 0.5, 1 and 6 were marked as LiNa-CC-0.5, LiNa-CC-1 and LiNa-CC-6, respectively. For comparison, Li-CC anodes and LiNa-alloy anodes were prepared using the similar method without the addition of sodium and carbon cloth, respectively. The average mass loading of LiNa alloy on CC is about 14.8 mg cm<sup>-2</sup>. Notably, with the increasing mass ratio of Na, the LiNa alloy is more difficult to be infused into the CC and pure sodium metal cannot be absorbed by the CC.

**Characterization.** Scanning electron microscopy (SEM) and energy disperse spectroscopy (EDS) were performed using a HITACHI S4700 electron microscopy. X-ray photoelectron spectroscopy (XPS) analysis was conducted using an ESCALAB 250 instrument. X-ray diffraction (XRD) measurements were performed on a D/max 2500 X-ray powder diffraction analyzer with Cu K $\alpha$  radiation (0.15406 nm).

**Electrochemical measurements.** CR2032 coin-type cells were assembled to investigate the electrochemical performance of LiNa-CC anode in Metal-Cu cells, symmetric cells and alkali Metal-Iodine (AM-I<sub>2</sub>) full batteries. All of the batteries were fabricated in the glove box (H<sub>2</sub>O, O<sub>2</sub> < 0.1 ppm). Bare Li foil, bare Na piece, Li-CC, LiNa-CC with various molar ratios were used both as working and counter electrode in the symmetric batteries. 1 M bis (trifluoromethane) sulfonimide lithium salt (LiTFSI) in 1,3-dioxolane (DOL)/1,2-dimethoxyethane (DME, 1:1 by

vol.) with 1 wt.% LiNO<sub>3</sub> and 1 M NaClO<sub>4</sub> in DME/DOL (1:1 by vol.) were employed as electrolyte. Celgard 2400 and glass fiber (Whatman GF-D) were used as separator. The test of obtained batteries were performed on a LANHE-CT2001A multichannel battery test instrument using a galvanostatic charge-discharge procedure at various current densities. All the cyclic voltammetry (CV) curves and electrochemical impedance spectroscopy (EIS) in a frequency range of 10<sup>-2</sup> ~10<sup>6</sup> Hz with 5 mV amplitude were measured on a SI 1287&1260 electrochemical measurement system (SOLARTRON CO.). All the electrochemical tests were performed at room temperature.

Iodine was used as cathode material in metal-iodine full batteries, which were assembled with LiNa anode, Celgard 2400 separator and iodine cathode. The as-assembled full batteries were investigated in Li (1 M LiTFSI in DOL/DEC, 1:1 by vol.) and Na (1 M NaClO<sub>4</sub> in DME/DOL, 1:1 by vol.) electrolyte, respectively. Iodine-carbon composites (I<sub>2</sub>-MC) were fabricated through a thermal diffusion method using our reported microporous carbon<sup>1</sup> as iodine host. Typically, iodine and MC were ground and sealed into a tube, then heated at 180 °C for 12 h. After washed with ethyl alcohol for several times and dried at 80 °C for 12 hours under vacuum, the I<sub>2</sub>@MC composites were prepared. For the preparation of iodine cathode, a slurry composed of I<sub>2</sub>@MC composites, Super P, polyvinylidene fluoride (PVDF) with a mass ratio of 8:1:1 was uniformly coated on carbon papers (current collector, TORAY). After drying at 80 °C for 12 hours under vacuum and cutting into 12 mm discs in diameter, the I<sub>2</sub>@MC cathode was prepared. The average iodine loading on carbon paper is 0.6 mg cm<sup>-2</sup>.

**Computational Details.** Density functional theory (DFT) calculations were performed using the DMol3 module in the Material Studio 6.0 software package. Based on the literature, a periodic 5 × 5 graphene supercell containing 50 carbon atoms was introduced to optimize the LiNa alloy-CC structure. A vacuum space between the graphene sheets in the z-direction was set to 20 Å, which is sufficiently large to avoid their interactions. All simulations were carried out

by using the Perdew-Burke-Ernzerhof (PBE) functional generalized gradient approximation (GGA) method. The k point grids were set as  $3 \times 3 \times 1$  for the Brillouin zone. The convergence tolerances of energies and maximum forces were set as  $10^{-5}$  Ha and  $0.002$  Ha/Å, respectively. The maximum displacement of  $0.005$  Å was chosen. The adsorption energies for bare Li/Na atom and LiNa alloy on the carbon matrix were calculated using the formula:  $E_{ads} = E_{12} - E_1 - E_2$ ,

where  $E_{ads}$  is the adsorption energy of the Li/Na atoms on LiNa-CC surfaces,  $E_1$  is the energy of Li/Na atoms,  $E_2$  is the total energy of the LiNa-CC, and  $E_{12}$  is the total energy of the Li/Na atom adsorbed on the LiNa-CC surface.

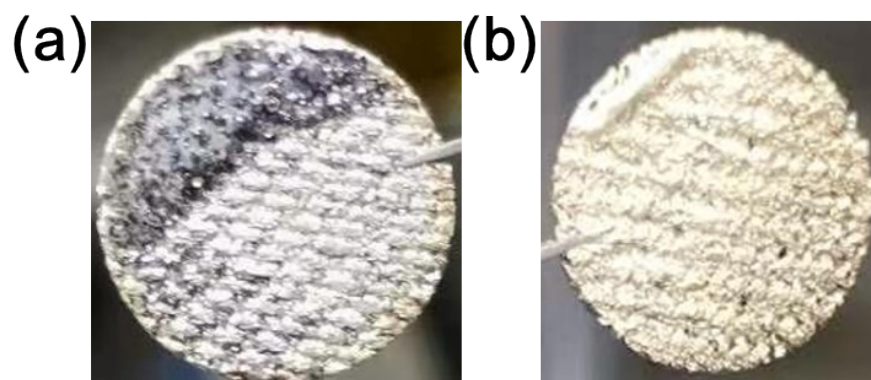


**Fig. S1** Optical photos of (a) silvery and (b) golden LiNa-CC anode.

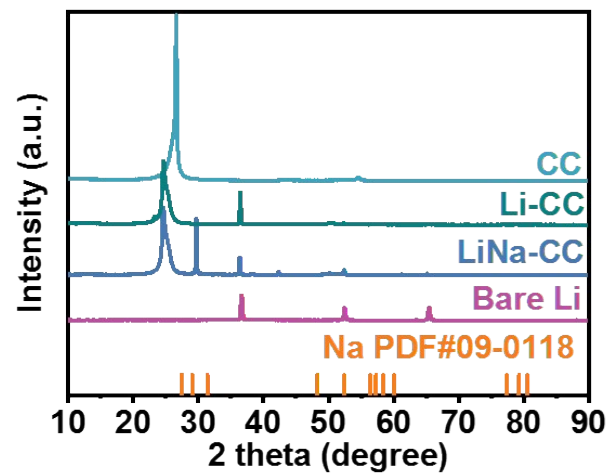


**Fig. S2** XRD patterns of various metal anodes.

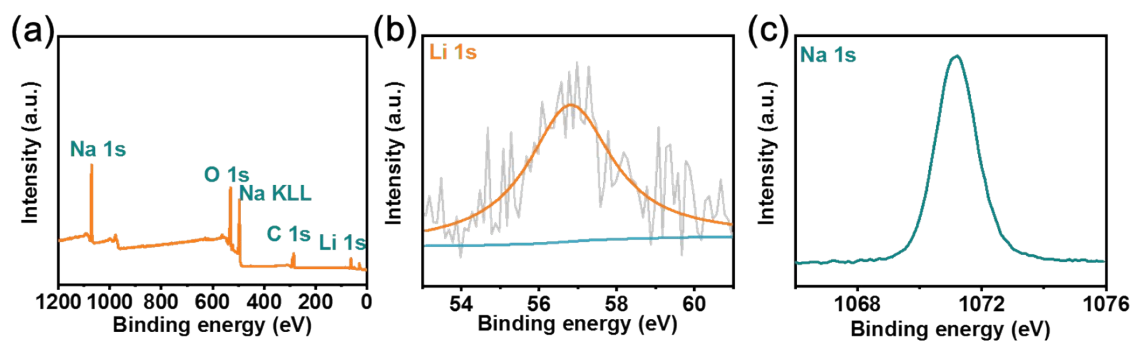


**Fig. S3** XPS spectra of (a) LiNa-CC anode. High-resolution XPS spectra of (b) Li and (c) Na.

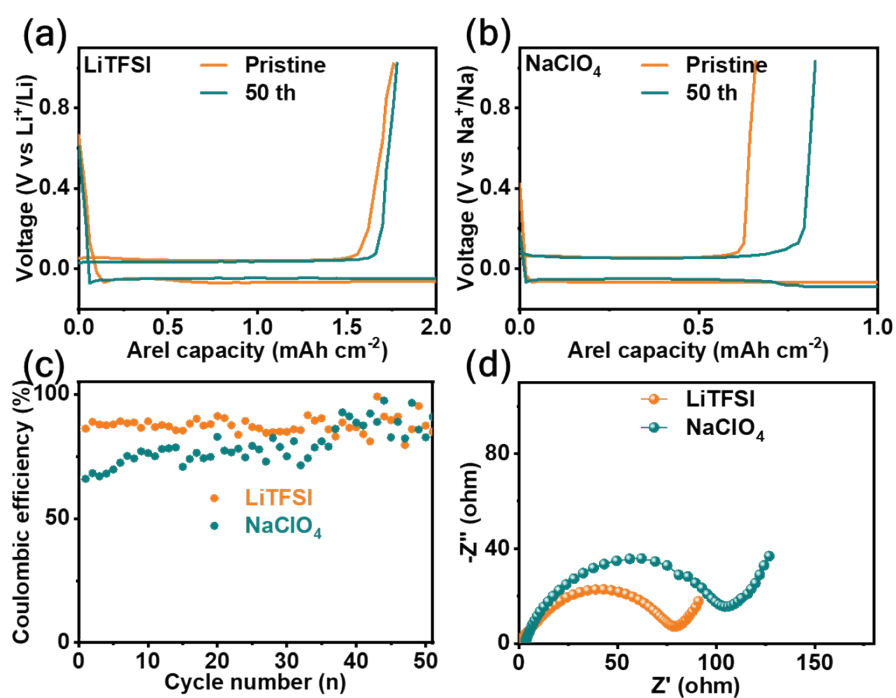


**Fig. S4** Electrochemical performance of LiNa-alloy anode in metal-Cu batteries. Voltage profiles testing in (a) LiTFSI and (b) NaClO<sub>4</sub> electrolyte at current density of 2 and 1 mA cm<sup>-2</sup>, respectively. (c) Coulombic efficiency and (d) Nyquist plots.

As shown in S4a and 4b, the LiNa-alloy anode exhibits a voltage hysteresis of 76 mV (125 mV) and an initial coulombic efficiency of 86.2% (65.9%) in LiTFSI (NaClO<sub>4</sub>) electrolyte. The coulombic efficiency shows distinct fluctuation after ~30 cycles (Fig. S4c), indicating its inferior stability to LiNa-CC electrode. As shown in Fig. S4d, the LiNa-alloy anode reveals charge transfer resistance ( $R_{ct}$ ) of 78  $\Omega$  and 105  $\Omega$  in LiTFSI and NaClO<sub>4</sub> electrolyte, respectively.

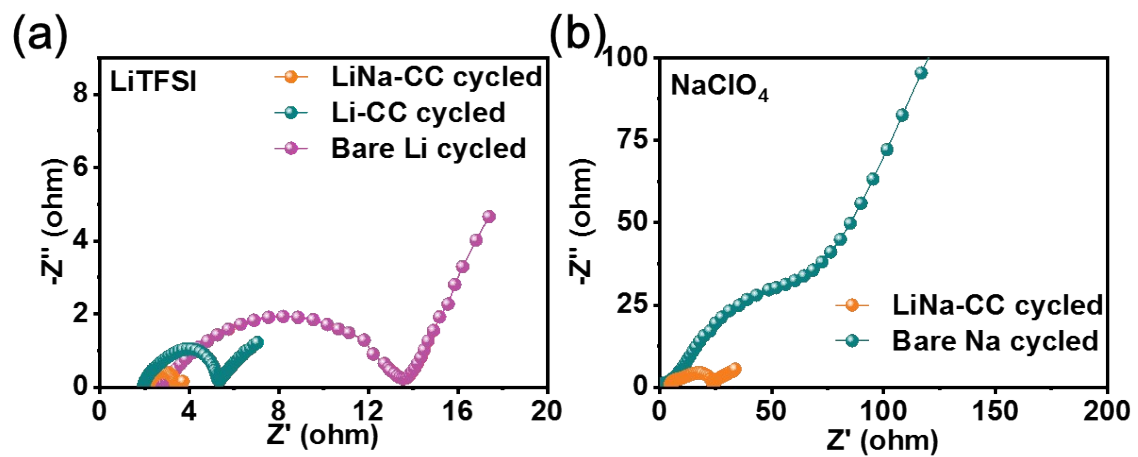


**Fig. S5** Nyquist plots of symmetric cells after cycling for (a) Li and (b) Na plating/stripping.

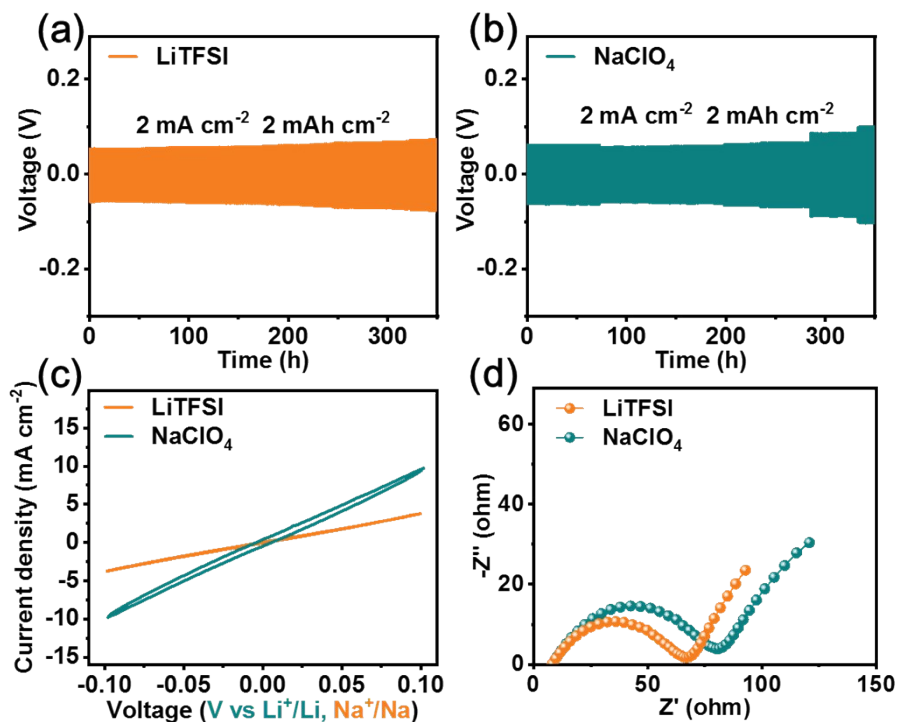


**Fig. S6** Electrochemical performance of LiNa-alloy anode in symmetric batteries. Voltage profiles testing in (a) LiTFSI and (b) NaClO<sub>4</sub> electrolyte at current density of 2 mA cm<sup>-2</sup>. (c) I-V curves and (d) Nyquist plots.

As shown in Fig. S6a and 6b, at current density of 2 mA cm<sup>-2</sup>, the LiNa-alloy anode exhibits an initial voltage hysteresis of ~118 and ~129 mV in LiTFSI and NaClO<sub>4</sub> electrolyte, respectively. After 350 h, the voltage hysteresis increases to ~158 and ~209 mV, respectively. As shown in Fig. S6c and S6d, the LiNa-alloy anode reveals the exchange current density of ~3.5 (9.6) mA cm<sup>-2</sup> and R<sub>ct</sub> of 67 and 81 Ω in LiTFSI and NaClO<sub>4</sub> electrolyte, respectively.

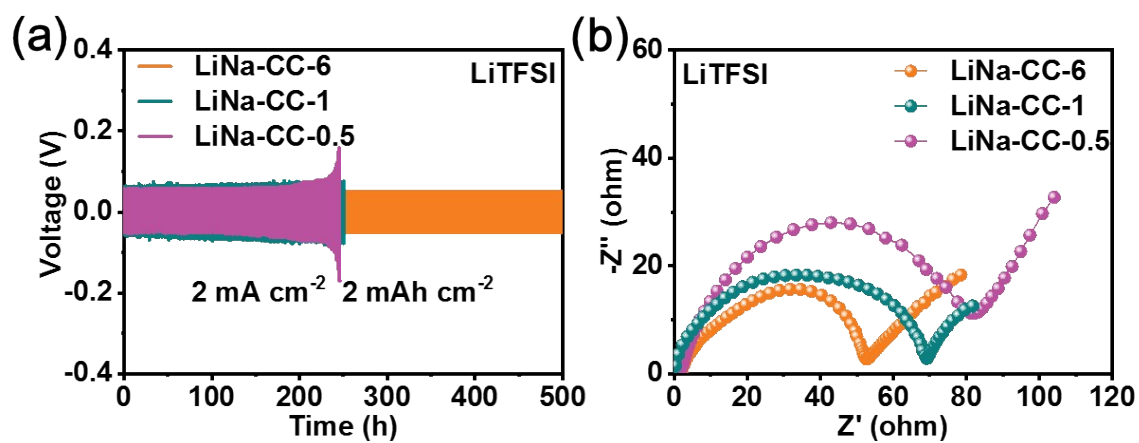


**Fig. S7** Electrochemical performance of LiNa-CC electrode with various Li/Na molar ratios on Li plating/stripping. (a) Galvanostatic charge/discharge curves and (b) Nyquist plots.

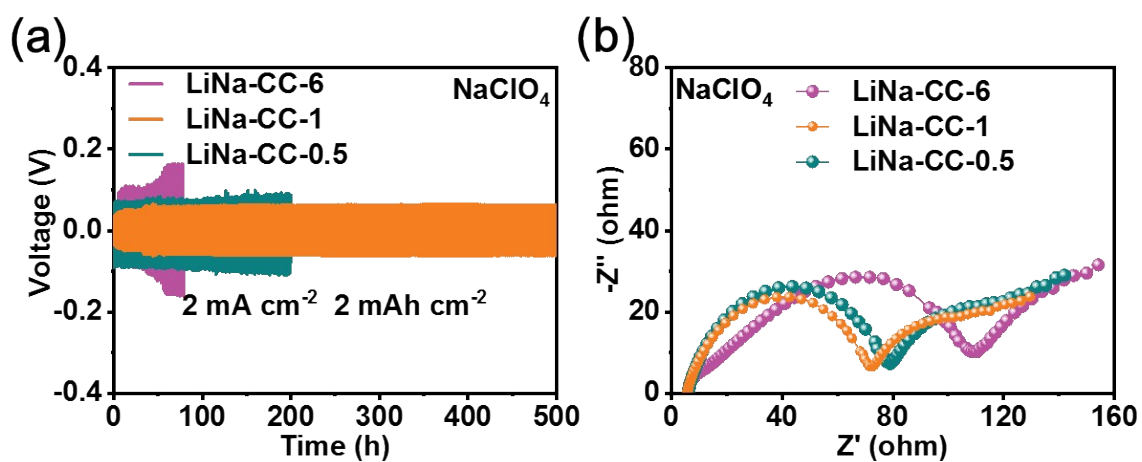


**Fig. S8** Electrochemical performance of LiNa-CC electrode with various Li/Na molar ratios on Na plating/stripping. (a) Galvanostatic charge/discharge curves and (b) Nyquist plots.

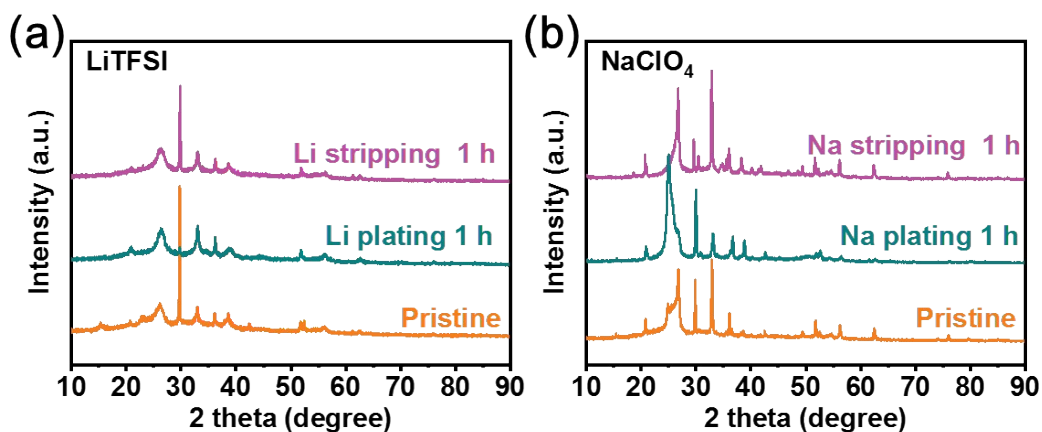


**Fig. S9** XRD patterns of LiNa-CC electrode at different discharge/charge states in symmetric batteries using (a) LiTFSI and (b) NaClO<sub>4</sub> electrolyte. Current density: 5 mA cm<sup>-2</sup>.

As shown in Fig. S9a, in LiTFSI electrolyte, LiNa-CC electrode reveals a decreased Na diffraction peak (~30 °) intensity after Li plating for 1 h (5 mA cm<sup>-2</sup>), suggesting the domination of Li ions in LiTFSI electrolyte. After the Li stripping for another 1 h, the LiNa-CC electrode shows a similar XRD pattern to the pristine state with an increase of Na diffraction peak, demonstrating the good reversibility and stability of LiNa-CC electrode. LiNa-CC also exhibits the similar stability for Na plating/stripping in NaClO<sub>4</sub> electrolyte (Fig. S9).

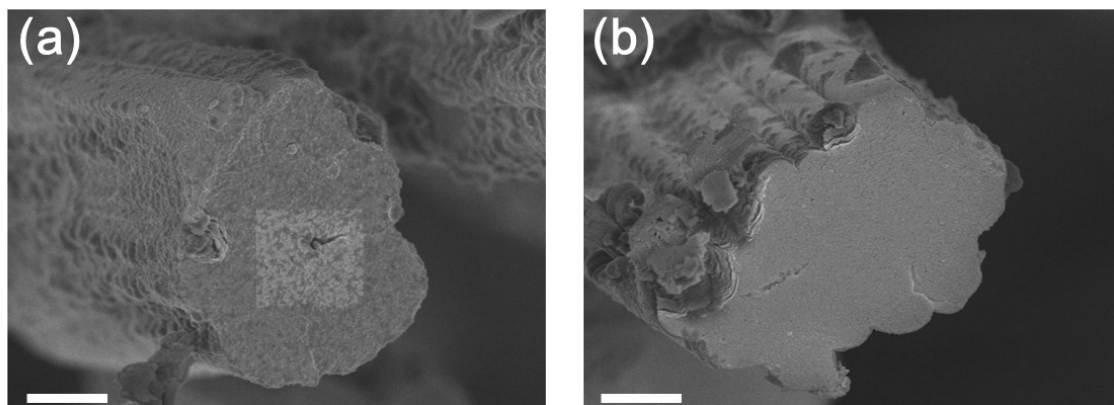


**Fig. S10** Cross-section SEM images of the LiNa-CC electrode after cycling in (a) LiTFSI and (b) NaClO<sub>4</sub> electrolyte, scale bars: 5  $\mu\text{m}$ .

As shown in Figure S10, after cycling at a current density of 2 mA cm<sup>-2</sup>, the LiNa-CC exhibits no obvious dendrites, indicating its good stability both in both LiTFSI and NaClO<sub>4</sub> electrolyte for Li and Na plating/stripping, respectively.

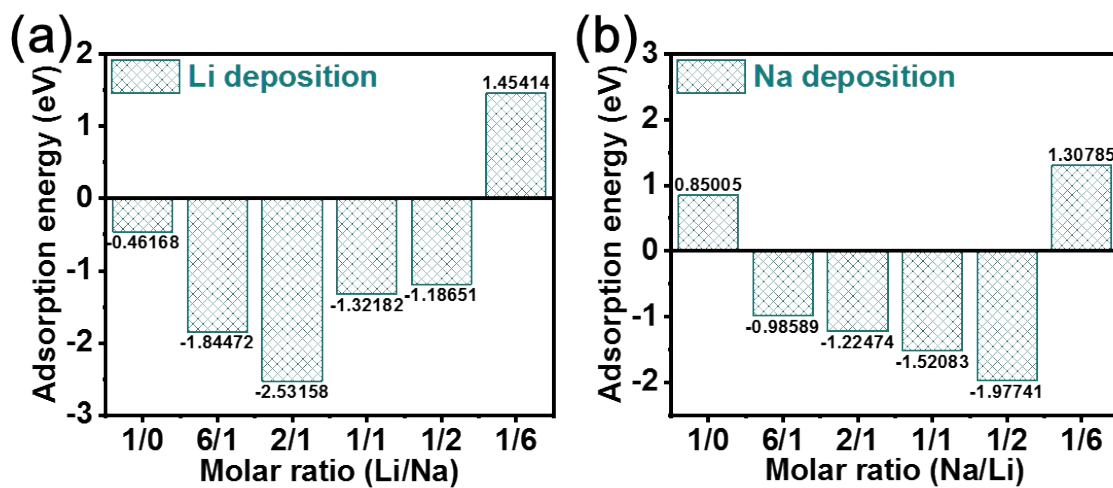


**Fig. S11** Adsorption energies of (a) Li and (b) Na atom on LiNa-CC electrode with various Li/Na molar ratios.

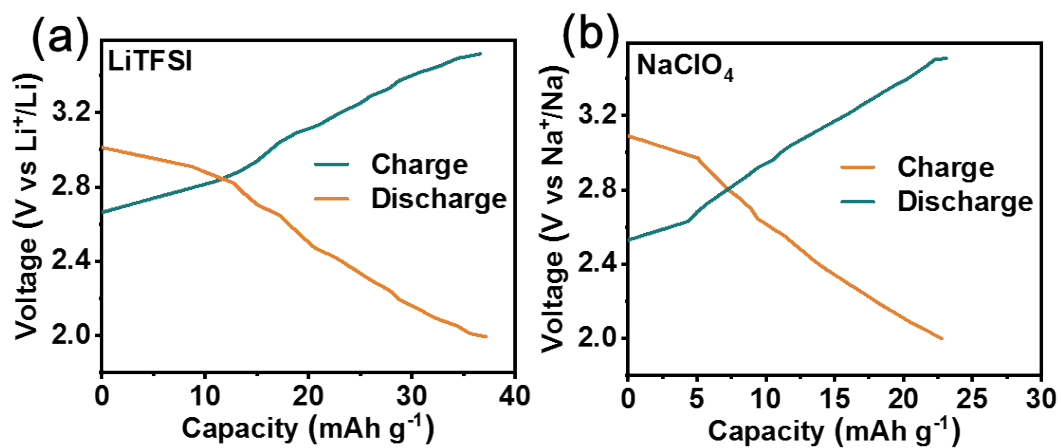


**Fig. S12** Capacitive contribution of the carbon matrix in (a) Li-I<sub>2</sub> and (b) Na-I<sub>2</sub> batteries.

As shown in the Figure S12, the MC carbon matrix exhibits the capacitive contribution of ~37.2 mAh g<sup>-1</sup> and 24.2 mAh g<sup>-1</sup> in LiTFSI and NaClO<sub>4</sub> electrolyte, respectively.

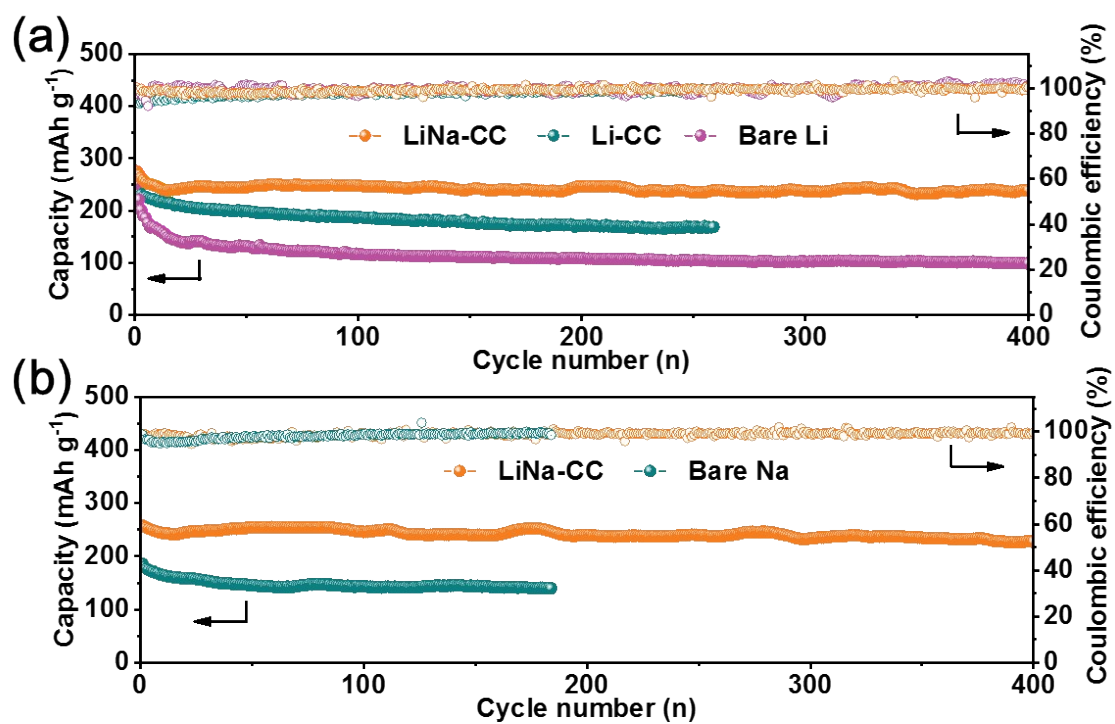


**Fig. S13** Cycling performance of various metal electrode in (a) Li-I<sub>2</sub> (2 C) and (b) Na-I<sub>2</sub> (0.5 C) batteries.

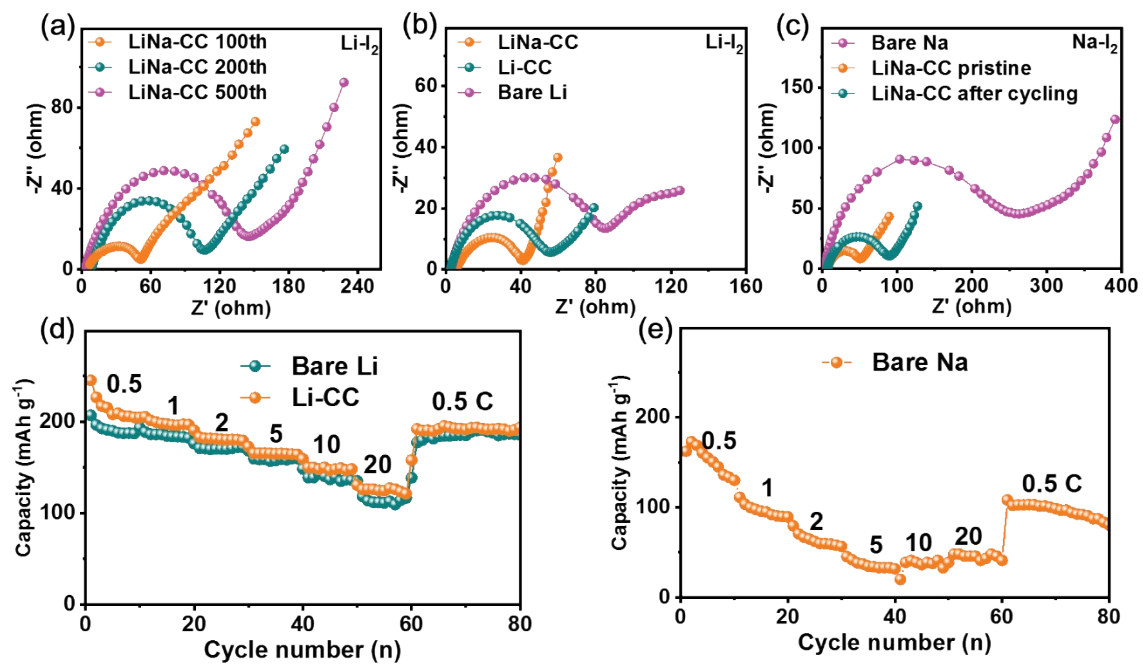


**Fig. S14** (a) Nyquist plots of metal-iodine batteries in different electrochemical state. Nyquist plots of metal-iodine batteries using various metal anodes in (b)  $\text{Li}$  and (c)  $\text{Na}$  ion electrolyte. (d) Rate performance of bare  $\text{Li}$  and  $\text{Li-CC}$ . (e) Rate performance of bare  $\text{Na}$ .

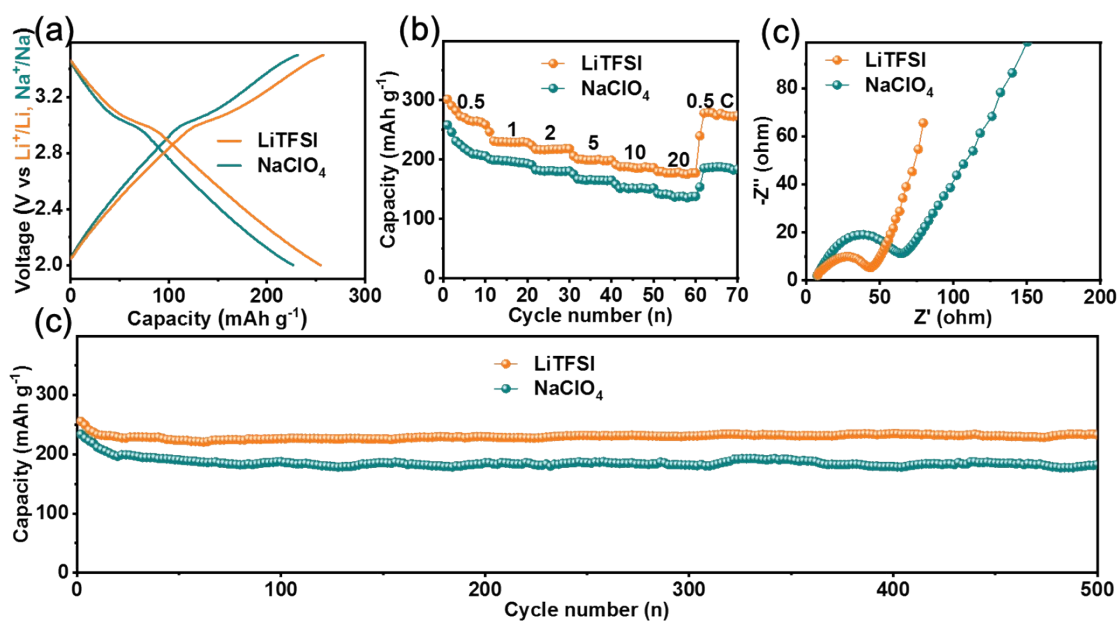


**Fig. S15** Electrochemical performance of LiNa-alloy anode in metal-iodine batteries. (a) Galvanostatic charge/discharge curves, (b) rate capability, (c) Nyquist plots and (d) long-term cycling stability.

As shown in Fig. S15a, the LiNa-alloy electrode displays a similar discharge and charge curves to LiNa-CC electrode both in LiTFSI and NaClO<sub>4</sub> electrolyte. At a current density of 20 C, the LiNa-alloy shows a capacity retention of 62.4% and 61.5% in LiTFSI and NaClO<sub>4</sub> electrolyte, respectively (Fig. S15b). At a current density of 2 C, LiNa-alloy electrode reveals a capacity retention of 90.9% and 85.8% after 500 cycles in LiTFSI and NaClO<sub>4</sub> electrolyte, respectively. As shown in Fig. S15c, the LiNa-alloy anode displays  $R_{ct}$  of 44  $\Omega$  and 65  $\Omega$  in LiTFSI and NaClO<sub>4</sub> electrolyte, respectively. Such electrochemical performance is inferior to LiNa-CC but better than bare Li and bare Na anode, suggesting the superiority of alloy strategy as well as the carbon cloth.

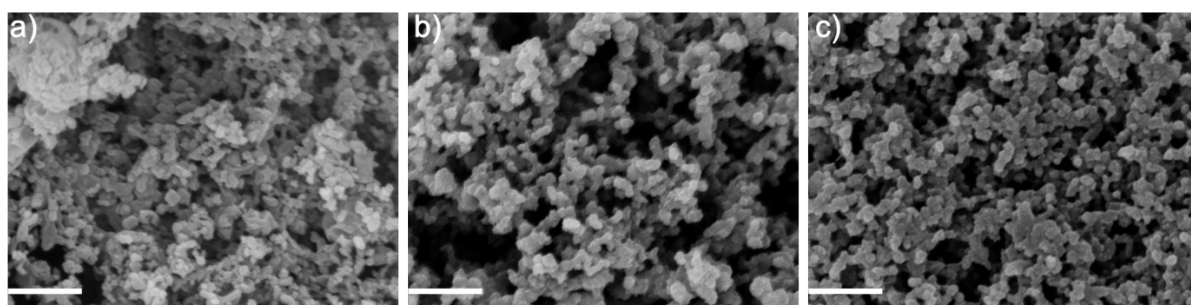


**Fig. S16** SEM images of the I<sub>2</sub>-MC cathode (a) fresh, after discharging in (b) Li and (c) Na based electrolyte (LiNa-CC anode). Scale bar: 500 nm.

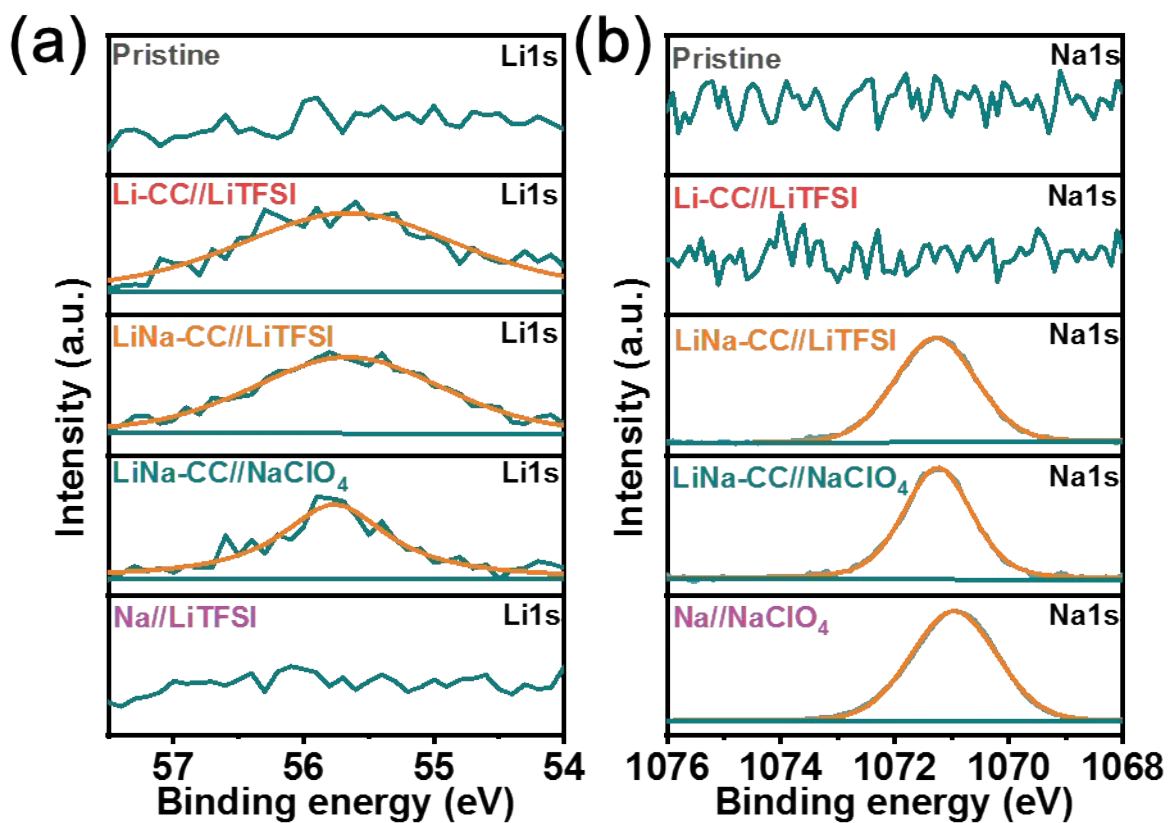


**Fig. S17** High resolution XPS spectra of (a) Li 1s and (b) Na 1s of iodine cathodes before and after cycling in different metal iodine batteries assembled with various metal anodes.

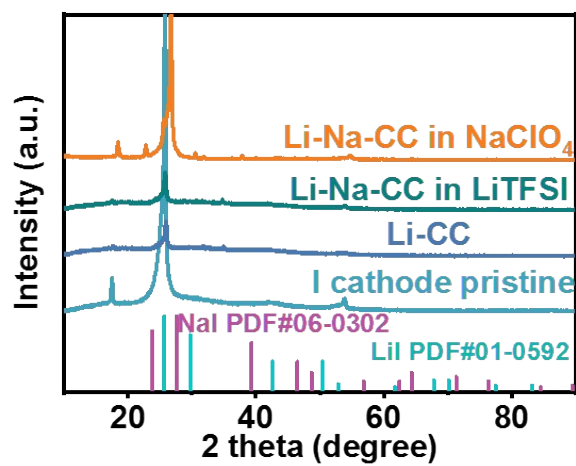


**Fig. S18** XRD patterns of iodine cathode cycled in different metal iodine batteries.

**Table S1.** Charge transfer resistance ( $R_{ct}$ ) of Metal-Cu cells.

Electrode	Electrochemical state/ $R_{ct}$ ( $\Omega$ )	Electrochemical state/ $R_{ct}$ ( $\Omega$ )
Bare Na	Pristine/257	50 <sup>th</sup> /463
Bare Li	Pristine/284	50 <sup>th</sup> /365
LiNa-CC//LiTFSI	Pristine/57	50 <sup>th</sup> /102
LiNa-CC//NaClO <sub>4</sub>	Pristine/54	50 <sup>th</sup> /114
LiNa// LiTFSI	Pristine/78	-
LiNa// NaClO <sub>4</sub>	Pristine/105	-

**Table S2.** Charge transfer resistance ( $R_{ct}$ ) of symmetric cells.

Electrode	Electrochemical state/ $R_{ct}$ ( $\Omega$ )	Electrochemical state/ $R_{ct}$ ( $\Omega$ )
Bare Li//LiTFSI	Pristine/150	5 <sup>th</sup> /13
Li-CC//LiTFSI	Pristine/112	5 <sup>th</sup> /5
LiNa-CC//LiTFSI	Pristine/38	5 <sup>th</sup> /3
LiNa-CC// NaClO <sub>4</sub>	Pristine/51	5 <sup>th</sup> /24
Bare Na/NaClO <sub>4</sub>	Pristine/203	5 <sup>th</sup> /138
LiNa// LiTFSI	Pristine/67	-
LiNa/NaClO <sub>4</sub>	Pristine/81	-

**Table S3.** Cycling performances of symmetric cells using various electrodes

Electrode	Current density (mA cm <sup>-2</sup> )	Cycling time (h)	Ref.
NPCC-Li	3	600	2
Li@CF	1	600	3
Li-Cu@Ni	3	208	4
Li@CFC	2	500	5
Au-Li@CFs	1	790	6
NG	1	180	7
Ag-Li@CF	1	400	8
LiNa-CC	40	800	<b>This work</b>
LiNa-CC	20	1650	<b>This work</b>

**Table S4.** Charge transfer resistance ( $R_{ct}$ ) of metal-iodine cells.

Electrode	Electrochemical state/ $R_{ct}$ ( $\Omega$ )	Electrochemical state/ $R_{ct}$ ( $\Omega$ )
Bare Li//LiTFSI	Pristine/84	100 <sup>th</sup> /9
Li-CC//LiTFSI	Pristine/56	100 <sup>th</sup> /5
LiNa-CC//LiTFSI	Pristine/42	100 <sup>th</sup> /51 200 <sup>th</sup> /106 500 <sup>th</sup> /144
Bare Na/NaClO <sub>4</sub>	Pristine/265	100 <sup>th</sup> /338
LiNa-CC/NaClO <sub>4</sub>	Pristine/52	100 <sup>th</sup> /91
LiNa//LiTFSI	Pristine/44	-
LiNa/NaClO <sub>4</sub>	Pristine/65	-

**Table S5.** Cycling stability and rate capacity of different metal-iodine batteries.

Battery	Capacity (mAh g <sup>-1</sup> ) Current density (C)	Capacity retention (%) Cycles Cycle rate (C)	Capacity retention (%) Rate (C)	Ref.
CC-I <sub>2</sub> //Li	301/0.5	64.8/300/0.5	56/5	9
Li@MPCP//Li	167.8/2	72.8/800/2	82/10	10
PVP-I <sub>2</sub> //Li	228.4/0.2	69.2/1100/2	68/5	11
CC-I <sub>2</sub> /Mxene//Li	330/0.5	85/1000/0.5	51/10	12
I <sub>2</sub> -HPCM-NP//Li	397/2C	76/2000/2	~ 71/10	13
rGO/LiI//Li	300/0.5 C	72/100/0.5	69/10	14
I <sub>2</sub> -HPCM-NP//Na	225/0.5 C	76/500/0.5	61/1	13
IGQDs-rGO//Na	173/0.5	87/500/0.5	54/5	15
I <sub>2</sub> -AC/Ti <sub>3</sub> C <sub>2</sub> T <sub>x</sub> //Li	162.6/2 C	78/1000/2	53/20	<b>16</b>
I <sub>2</sub> -MC//LiNa-CC	398/0.5	85/2000/5	65/20	<b>This work</b>
I <sub>2</sub> -MC//LiNa-CC	264/0.5	83/2000/5	64/20	<b>This work</b>

## REFERENCES

- 1 T. Li, D. Yu, J. Liu, and F. Wang, *ACS Appl. Mater. Interfaces*, 2019, **11**, 37559-37566.
- 2 K. Li, Z. Hu, J. Ma, S. Chen, D. Mu, and J. Zhang, *Adv. Mater.*, 2019, **31**, 1902399.
- 3 L. Tao, A. Hu, Z. Yang, Z. Xu, C.-E. Wall, A.-R. Esker, Z. Zheng, and F. Lin, *Adv. Funct. Mater.*, 2020, **30**, 2000585.
- 4 L. Lu, Y. Zhang, Z. Pan, H. Yao, F. Zhou, and S.-H. Yu, *Energy Storage Mater.* 2017, **9**, 31.
- 5 W. Deng, W. Zhu, X. Zhou, and Z. Liu, *Energy Storage Mater.*, 2018, **15**, 266.
- 6 J. Xiang, L. Yuan, Y. Shen, Z. Cheng, K. Yuan, Z. Guo, Y. Zhang, X. Chen, and Y. Huang, *Adv. Energy Mater.*, 2018, **8**, 1802352.
- 7 R. Zhang, X. R. Chen, X. Chen, X. B. Cheng, X. Q. Zhang, C. Yan, and Q. Zhang, *Angew. Chem. Int. Ed.*, 2017, **56**, 7764.
- 8 R. Zhang, X. Chen, X. Shen, X.-Q. Zhang, X.-R. Chen, X.-B. Cheng, C. Yan, C.-Z. Zhao, and Q. Zhang, *Joule*, **2018**, *2*, 764.
- 9 K. Li, S. Chen, S. Chen, X. Liu, W. Pan, J. Zhang, *Nano Res.*, 2018, **12**, 549-555.
- 10 Z. Wu, J. Xu, Q. Zhang, H. Wang, S. Ye, Y. Wang, and C. Lai, *Energy Storage Mater.*, 2018, **10**, 62-68.
- 11 Z. Meng, H. Tian, S. Zhang, X. Yan, H. Ying, W. He, C. Liang, W. Zhang, X. Hou, and W. Han, *ACS Appl. Mater. Interfaces*, 2018, **10**, 17933-17941.
- 12 X. Tang, D. Zhou, P. Li, X. Guo, C. Wang, F. Kang, B. Li, and G. Wang, *ACS Cent. Sci.*, 2019, **5**, 365-373.
- 13 K. Lu, Z. Hu, J. Ma, H. Ma, L. Dai, and J. Zhang, *Nat. Commun.*, 2017, **8**, 527.
- 14 S. Kim, S. K. Kim, P. Sun, N. Oh, P. V. Braun, *Nano Lett.*, 2017, **17**, 6893-6899.
- 15 D. Gong, B. Wang, J. Zhu, R. Podila, A. M. Rao, X. Yu, Z. Xu, and B. Lu, *Adv. Energy Mater.*, 2017, **7**, 1601885.
- 16 C. Sun, X. Shi, Y. Zhang, J. Liang, J. Qu, and C. Lai, *ACS Nano*, 2020, **14**, 1176-1184.